CONF-9109330--1

DE92 005161

Transverse and Forward Energy Measurements in Nucleus-Nucleus Collisions at 60 and 200 GeV/nucleon

WA80 Collaboration

S. P. Sorensen[b,f], R. Albrecht[a], T. C. Awes[b], C. Baktash[b], P. Beckmann[c,1], F. Berger[c], R. Bock[a], G. Claesson[d], G. Clewing[c], L. Dragon[c], A. Eklund[d], R. L. Ferguson[b], A. Franz[e,f,1], S. Garpman[d], R. Glasow[c], H. A. Gustafsson[d], H. H. Gutbrod[a], J. Idh[d], P. Jacobs[e], K.-H. Kampert[c], B. W. Kolb[a], P. Kristiansson[d], I. Y. Lee[b], H. Loehner[c,2], I. Lund[a,2], F. E. Obenshain[b], A. Oskarsson[d], I. Otterlund[d], T. Peitzmann[c], S. Persson[d], F. Plasil[b], A. M. Poskanzer[e], M. Purschke[c], H.-G. Ritter[e], S. Saini[b], R. Santo[c], H. R. Schmidt[a], T. Siemiarczuk[a,3], E. Stenlund[d], M. L. Tincknell[b,4], and G. R. Young[b]

[a] *Gesellschaft für Schwerionenforschung, Darmstadt, Federal Republic of Germany*
[b] *Oak Ridge National Laboratory, Oak Ridge, Tennessee, USA*
[c] *University of Münster, Münster, Federal Republic of Germany*
[d] *University of Lund, Lund, Sweden*
[e] *Lawrence Berkeley Laboratory, Berkeley, California, USA*
[f] *University of Tennessee, Knoxville, Tennessee, USA*

– Invited Paper –
Hadron Structure '91
Stara Lesna, Czechoslovakia
September 16-20, 1991

I. Introduction

The aim of the high energy heavy ion programs at the SPS and AGS accelerators is to study nuclear matter under conditions of extremely high densities and temperatures[5]. Theoretical calculations[5] predict that under such conditions hadronic matter might undergo a phasetransition to a new form of matter, the quark-gluon plasma or QGP, in which quarks and gluons are deconfined over an extended volume. A broad spectrum of possible plasma signatures has been suggested[5]. An unfortunate common characteristic of most of these signatures is the necessity to distinguish them from the background created by ordinary hadronic processes. A thorough understanding of the reaction mechanisms in high energy heavy ion

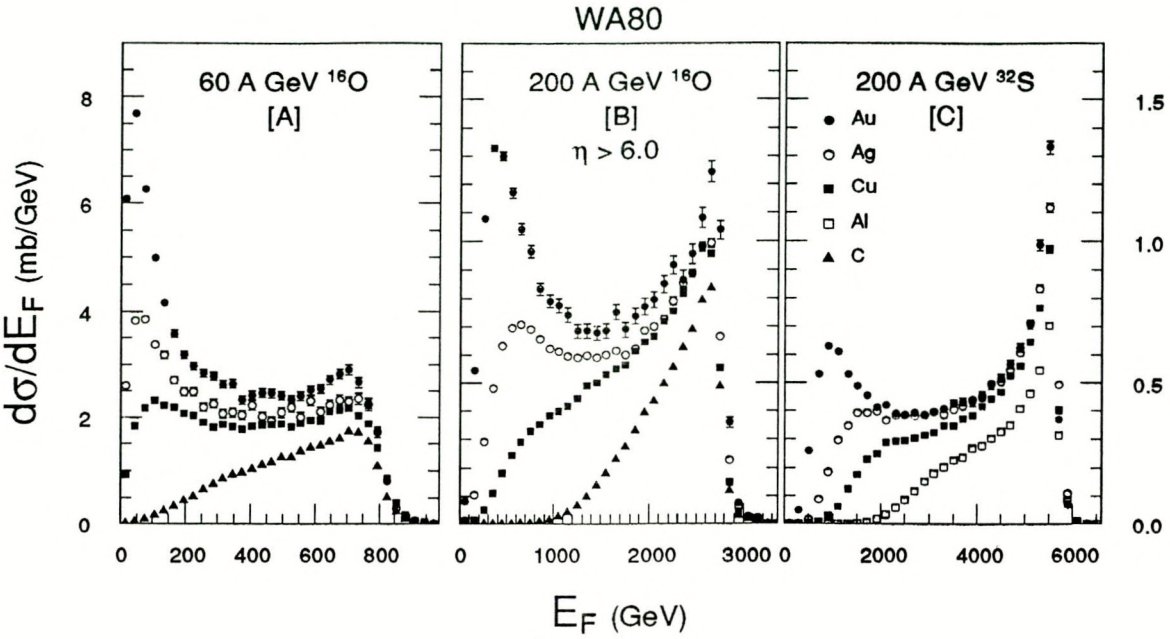

Figure 1. Forward energy spectra for heavy ion reactions induced by A) 60 A GeV ^{16}O, B) 200 A GeV ^{16}O, and C) 200 A GeV ^{32}S. The error bars reflect the statistical errors. At energies below 700 GeV, 2600 GeV, and 5500 GeV for A, B and C, respectively, the spectra are corrected for distortions caused by trigger cuts and background events. The vertical scales in B) and C) are identical.

collisions is, therefore, an important prerequisite in any QGP search. Global event quantities like the transverse energy E_T, the forward energy E_F, and the charged particle multiplicity have proven to be valuable tools for obtaining this understanding of the reaction mechanisms[6-13].

In this contribution to the Hadron Structure 1991 Conference will be presented results concerning the transverse energy and forward energy extracted from WA80's calorimeters in a series of measurements using beams of ^{16}O and ^{32}S bombarding nuclear targets. For further details concerning the experimental setup and the data analysis, please refer to Ref. 14 and references therein.

II. Forward energy

The energy deposited in the Zero-Degree Calorimeter is called the forward energy, E_F, by WA80 and corresponds to the sum of the energy of all particles with scattering angles smaller than $\approx 0.3^o$ ($\eta > 6$). The E_F-spectra for both ^{16}O- and ^{32}S-induced reactions shown in Fig. 1 can be qualitatively understood from simple arguments based on the nuclear overlap geometry. The lowest values of E_F will correspond to the most central collisions. The importance of the nuclear geometry in the determination of the shape of energy-spectra in high energy nuclear collisions can be

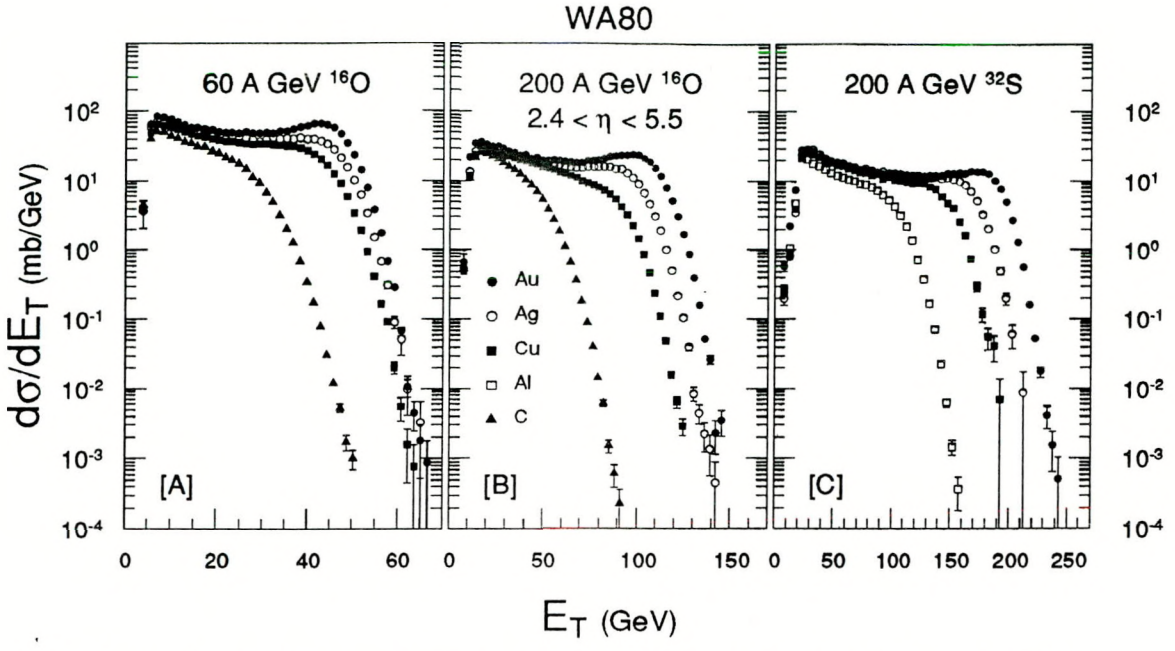

Figure 2. Transverse energy spectra for heavy ion reactions induced by A) 60 A GeV ^{16}O, B) 200 A GeV ^{16}O, and C) 200 A GeV ^{32}S. The error bars reflect the statistical errors. At energies above 8 GeV, 20 GeV, and 30 GeV for A, B, and C, respectively, the spectra are corrected for distortions caused by background events.

illustrated by the following scaling law. The shape of the E_F-spectra at 200 A GeV scales approximately with the geometric ratio R_t/R_p or stated more precisely

$$\begin{aligned} \frac{d\sigma}{de} &\approx \sigma_{tot} \cdot f(e, \frac{R_t}{R_p}) \\ e &= E_F/E_{beam} \\ \sigma_{tot} &= \pi r_o^2 (A_t^{1/3} + A_p^{1/3})^2 \end{aligned} \tag{1}$$

Examples of this scaling law are the similarities between the E_F-spectra for O + Ag and S + Au, where the ratios between the radii are 1.89 and 1.83, respectively, and the spectra for O + C and S + Al with ratios of 0.91 and 0.94, respectively.

III. Transverse energy

The ^{16}O- and ^{32}S-induced E_T-spectra, as shown in Fig. 2, share a set of features which, apart from trigger bias, can also be understood primarily from the nuclear overlap geometry. At very low energies ($E_T < 0.1\ E_T^{max}$) the spectra fall off due to the trigger bias against the most peripheral events. Spectra with less peripheral bias, as measured by NA34[9] and NA35[6], show a dramatic increase at low E_T. Above $\approx 0.2\ E_T^{max}$ the spectra decrease either slowly or are approximately constant. For

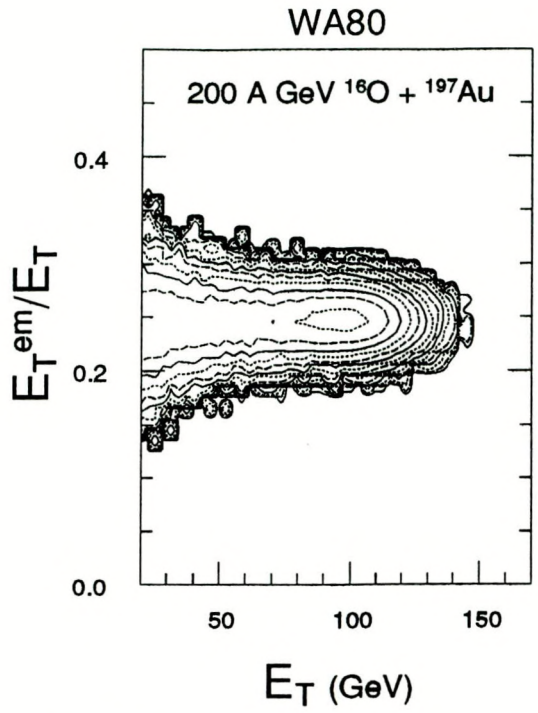

Figure 3. Contour plot of E_T^{em}/E_T vs. E_T for $2.4 < \eta < 5.5$. The outermost contour is set just below the 1 count/channel level and each successive contour corresponds to an increase of the yield/channel by a factor of 2. The spectrum has not been smoothed.

the heaviest targets this plateau ends in a bump which is followed by a rapidly falling tail of Gaussian shape[15]. As discussed in Ref. 8 E_T and E_F display a narrow anticorrelation. This leads to an interpretation of the E_T-spectra in terms of decreasing impact parameter for increasing E_T. The long plateau corresponds to reactions in which successively more of the projectile overlaps the target, and the bump can be identified with central collisions in which the entire projectile is engulfed by the target as discussed in Section II. The Gaussian tail at large E_T values is observed to extend over more than 5 decades. An earlier analysis[15] suggests that this tail is largely due to fluctuations in the number of participating nucleons rather than to variations in the E_T produced per emitting source.

A comparison between the ^{16}O- and ^{32}S-induced E_T-spectra at 200 A GeV shows that in the tail region the ratio between E_T for S+Au and O+Au is ≈ 1.65. This value is, however, strongly dependent on the particular η-interval over which E_T is integrated. For the interval $-0.1 < \eta < 2.9$ NA34[10] finds a ratio of ≈ 1.50. In Section IV it will be demonstrated how these different ratios are a simple consequence of the decreasing dependence on projectile mass at decreasing η-values.

The segmentation of the calorimeters together with a knowledge of the response of the calorimeters to various particles makes it possible to separate the observed E_T into electromagnetic $E_{T,em}$ and hadronic $E_{T,had}$ components based on the signals

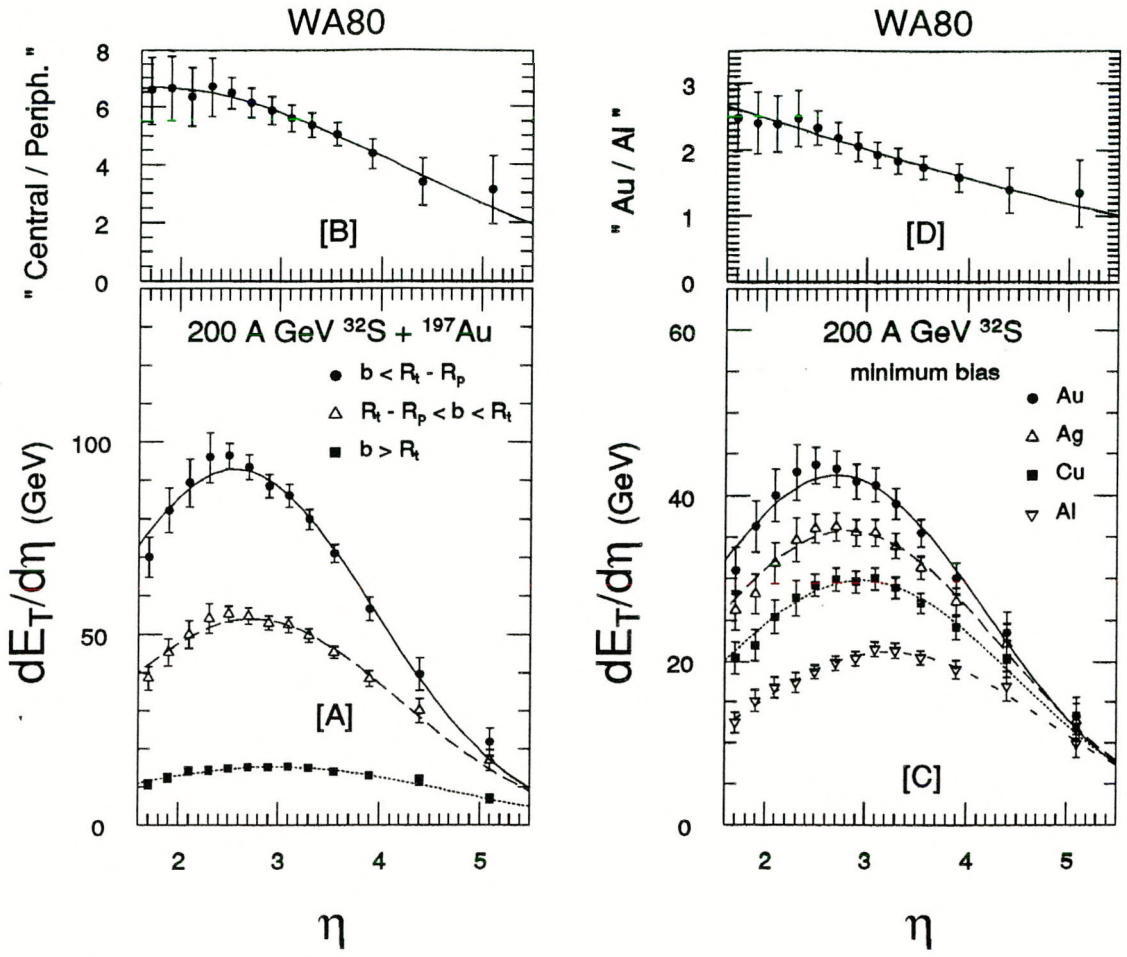

Figure 4. A) Dependence of $dE_T/d\eta$ for 200 A GeV ^{32}S + ^{197}Au on impact parameter. The 3 distributions correspond from top to bottom to central, intermediate, and peripheral collisions. The curves drawn through the data points in Figs. 4A-5A are Gaussian fits. B) Ratio between the $dE_T/d\eta$-distribution for central and peripheral events. C) Target dependence of $dE_T/d\eta$ in 200 A GeV ^{32}S-induced minimum bias collisions. D) Ratio between $dE_T/d\eta$-distributions for ^{197}Au and ^{27}Al targets.

recorded in the electromagnetic (S_{em}) and hadronic (S_{had}) longitudinal sections of WA80's MIdRApidity Calorimeter, MIRAC. Investigations of more than 2 million events of S_{em} vs. S_{had} revealed no exotic events with ratios S_{em}/S_{had} deviating dramatically from the values predicted by the event generators, like *e.g.*"Centauro" events[16] with abnormal low electromagnetic energy content. This is illustrated in Figure 3, which shows a contour plot of the ratio $E_T{}^{em}/E_T$ vs. E_T. Note the symmetry of the distribution along the ordinate and the absence of any group of events with abnormal electromagnetic content.

IV. $dE_T/d\eta$ distributions

In this section the dependence of the $dE_T/d\eta$-distributions on impact param-

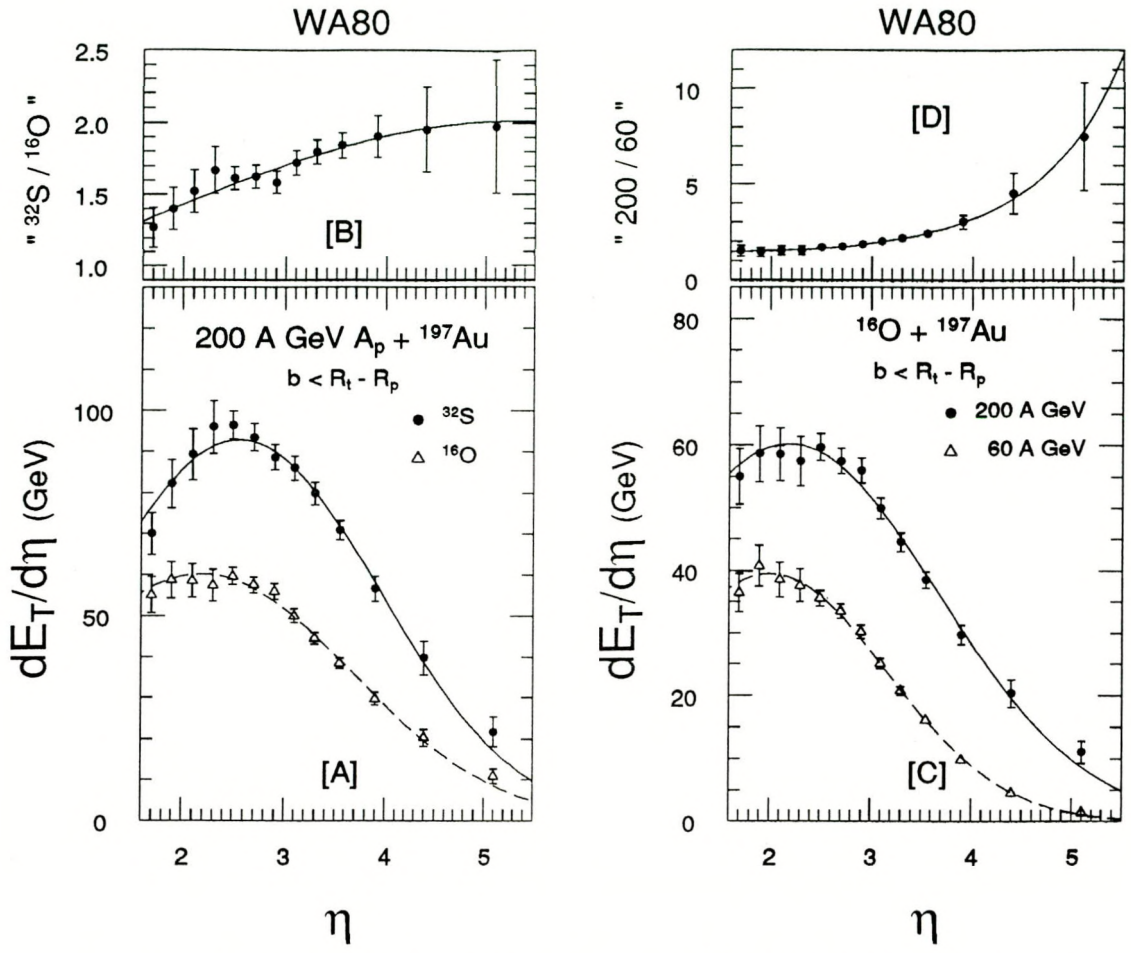

Figure 5. A) Projectile dependence of $dE_T/d\eta$ in 200 A GeV A_p + ^{197}Au central collisions. B) Ratio between the $dE_T/d\eta$-distributions for ^{32}S- and ^{16}O-induced reactions. C) $dE_T/d\eta$-distributions for 60 A and 200 A GeV ^{16}O + ^{197}Au central collisions. D) Ratio between $dE_T/d\eta$-distributions for 200 A GeV and 60 A GeV. See Fig. 4 for further details.

eter, target, projectile, and beam energy will be discussed. All of the $dE_T/d\eta$-distributions presented for a particular event class have been fitted with Gaussian functions. These fits are also presented as curves through the datapoints in the Figs. 4-5. The 3 free parameters in these fits: 1) the height of the distribution $dE_T/d\eta|_{max}$, 2) the centroid $\overline{\eta}$, and 3) the standard deviation σ_η are presented in tables in Ref. 14. The use of a Gaussian fit in order to calculate $\overline{\eta}$ and σ_η was necessary since WA80 does not have full η-coverage. The χ^2 per degree of freedom for the fits were typically ranging from 0.3 to 0.5. Since additional free parameters did not decrease the χ^2 it was concluded, that the characterization of each $dE_T/d\eta$-distribution by a Gaussian shape with 3 free parameters exhausts the full information content in the measured distributions.

The dependence of the $dE_T/d\eta$-spectra on the impact parameter of the collision

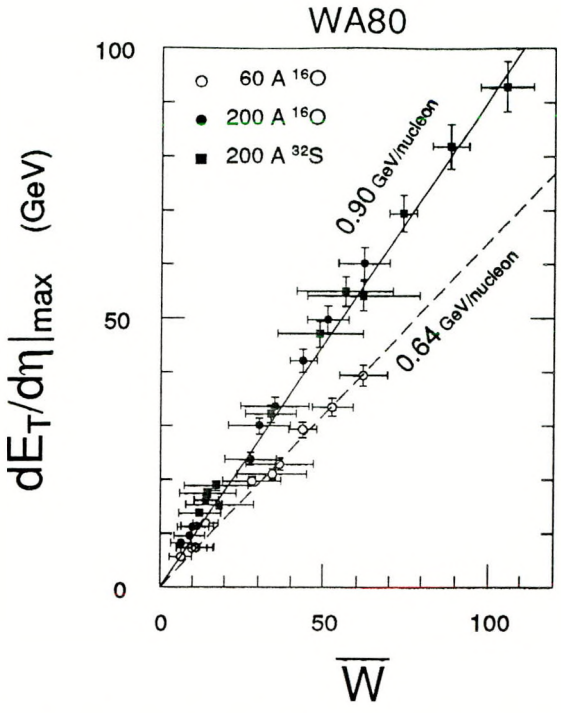

Figure 6. Maximum value of the $dE_T/d\eta$-distributions as a function of the total average number of participants $\overline{W}$. The straight lines show linear fits through the origin to the data points at 60 A and 200 A GeV, respectively.

is shown in Fig. 4A. The 3 distributions correspond to central, intermediate, and peripheral collisions as defined in Ref. 14. For the system 200 A GeV ^{32}S + ^{197}Au shown in Fig. 4 the following impact parameter dependence is observed: a) $dE_T/d\eta|_{max}$ increases from 15 GeV for peripheral collisions to 93 GeV in central collisions, b) the centroid decreases from $\eta = 3.0$ to $\eta = 2.6$ and c) the standard deviation decreases from $\sigma = 1.7$ to $\sigma = 1.4$. As seen in Fig. 4B the $dE_T/d\eta$ increases much more rapidly at backward rapidities than at forward rapidities as a function of increasing centrality.

The dependence of $dE_T/d\eta$ on target mass is illustrated in Fig. 4C. Qualitatively the effects of increasing the target mass are very similar to decreasing the impact parameter as can be seen by comparing Figs. 4A and 4C. The η-positions of the maxima of the distributions decrease from 3.2 for ^{27}Al to 2.7 for ^{197}Au.

A point of some controversy has been the projectile mass dependence of E_T in central collisions. As can be seen from Fig. 5A this dependence is strongly rapidity dependent. In the projectile rapidity region $dE_T/d\eta$ increases approximately proportional with the projectile mass, A_p, whereas in the target rapidity region the dependence on A_p is much weaker. The scaling factor of 1.67 for E_T between ^{32}S- and ^{16}O-induced reactions quoted in Section III corresponds to the average ratio between the two spectra in Fig. 5A in the interval $2.4 < \eta < 5.5$. The scaling factor of 1.50 measured by NA34 with a coverage of $-0.1 < \eta < 2.9$ also seems reasonable

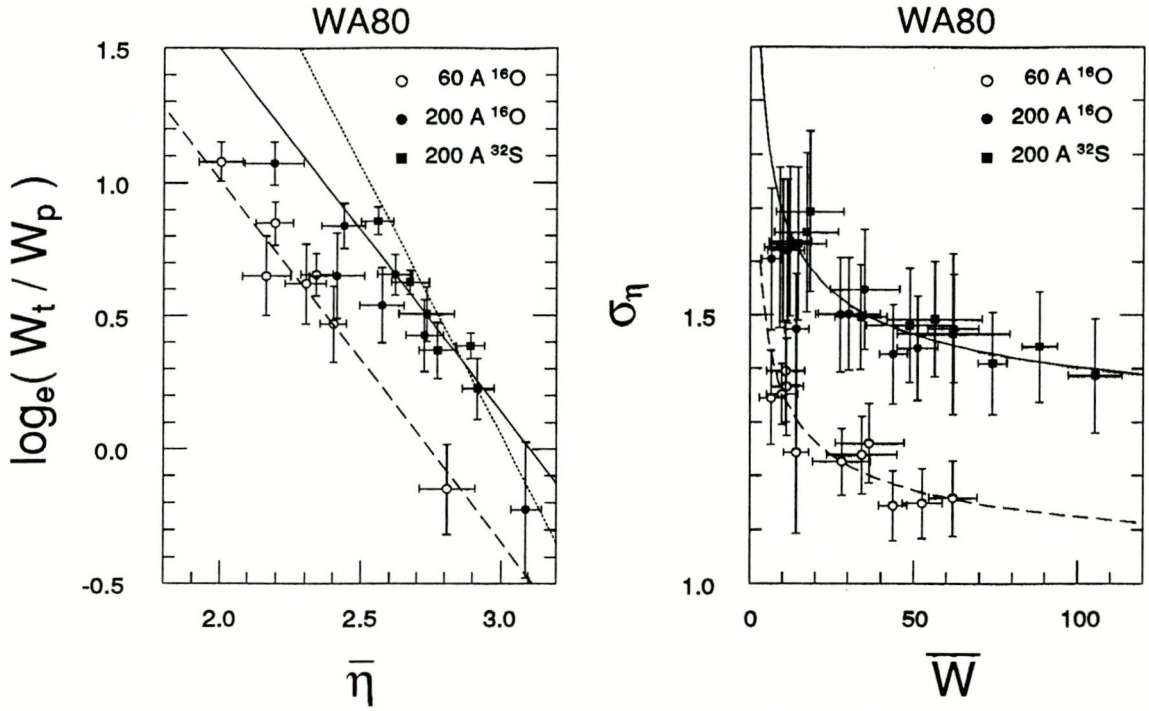

Figure 7. A) Centroid $\overline{\eta}$ as a function of the ratio between target and projectile participants. The dotted line shows the expected behaviour at 200 A GeV based on equation (2). The solid and dashed lines show the linear fits to the data at 200 A GeV and 60 A GeV, respectively. B) Standard deviation σ_η the $dE_T/d\eta$-distributions as a function of the total number of participants.

based on the decrease of the scale factor in Fig. 5B from 1.65 at $\eta = 3.0$ to 1.3 at $\eta = 1.6$

The dependence of $dE_T/d\eta$ on bombarding energy is illustrated in Fig. 5C for 60 A and 200 A GeV ^{16}O + ^{197}Au collisions. The maximum value of $dE_T/d\eta$, the centroid and the standard deviation are all seen to increase as functions of $\sqrt{s}$. The scaling factor shown in Fig. 5D is seen to increase dramatically at forward pseudo-rapidities. Note, that although the distribution is wider at 200 A GeV than at 60 A GeV, there is no evidence for a mid-rapidity plateau as assumed in the Bjorken model[17]. This is not surprising in view of a) the narrowness of such a plateau even at ISR energies of $\sqrt{s} = 53$ GeV for p+p, where the plateau only spans 3-4 rapidity-units, and b) the larger number of binary nucleon-nucleon collisions in heavy-ion reactions which will tend to make the $dE_T/d\eta$ distribution more focused around mid-rapidity.

The behaviour of the quantities $dE_T/d\eta|_{max}$, $\overline{\eta}$, and σ_η extracted from the Gaussian fits to the $dE_T/d\eta$-distributions are illustrated in the Figs. 6-7. The behaviour of these quantities can be well described within a participating nucleon model[11]. From the forward energy, E_F, the impactparameter b can be estimated on an event-by-event basis to within $\pm$ 1 fm, and from b and the projectile- and target masses

the average number of participating nucleons can be estimated via Glauber theory.

Fig. 6 shows the $dE_T/d\eta|_{max}$ values plotted as a function of the total number of participants $\overline{W}$. In accordance with an earlier observation by WA80[18] the $dE_T/d\eta|_{max}$ is approximately linearly proportional to the average number of participants $\overline{W}$ with the coefficient of proportionality equal to 0.64 and 0.90 GeV/nucleon at 60 A and 200 A, respectively. The increase of $dE_T/d\eta|_{max}$ in Figs. 4 as a function of decreasing impact parameter or increasing target mass is therefore a simple consequence of the increase of $\overline{W}$.

The variation of the centroid $\overline{\eta}$ is more complicated. $\overline{\eta}$ will move backwards for increasing centrality, increasing target mass, decreasing projectile mass or decreasing bombarding energy. All of these variations can be understood from the following approximate formula for the effective CM rapidity, y_{cm}

$$\overline{\eta} \approx y_{cm} \approx \frac{1}{2}(y_p + y_t + \log\frac{W_p}{W_t}) \tag{2}$$

y_p and y_t are the projectile and target rapidities, respectively. Eq. (2) is based on the assumption that all of the W_p projectile participants interact collectively with all of the W_t target participants. Even if this is not the case, the above formula seems to qualitatively predict the correct behaviour of $\overline{\eta}$ as can be seen from the dotted line in Fig. 7. For decreasing impact parameter in an asymmetric projectile-target combination ($A_p < A_t$) the ratio W_p/W_t will decrease from ≈ 1 to $\approx \sqrt{A_p/A_t}$ for the most central collisions. This will, according to Eq. (2), cause $\overline{\eta}$ to decrease as observed in the data. Similarly, an increasing target mass or decreasing projectile mass will cause $\log(W_p/W_T)$ to decrease, and finally an increase in $\sqrt{s}$ will increase $y_p + y_t$ causing $\overline{\eta}$ to increase as also observed in the data. It is, however, clear from observing the slope of the dotted line in Fig. 7 that Eq. (2) is not able to quantitatively predict the correct behaviour, especially for heavy targets where the experimental centroids are situated at smaller rapidities than predicted by Eq. (2). A possible explanation for this deviation could be the increased importance of rescattering effects for heavy targets, which will tend to make the effective number of target participants larger and thereby move the effective center-of-mass backwards as observed in the data.

The width of the $dE_T/d\eta$-distributions, as shown in Fig. 7B, becomes narrower for more central collisions. This behaviour is most likely caused by an increase in stopping, since the participants have to penetrate more nuclear matter in central collisions causing them to have final rapidities closer to that of the effective center-of-mass system and causing a larger fraction of the produced particles to be emitted near mid-rapidity.

The information shown in Figs. 6-7 can be used[14] to parameterize the $dE_T/d\eta$-distribution at a particular impactparameter b in terms of a Gaussian distribution

as follows:

$$\frac{dE_T}{d\eta}(b) = H \exp\left\{-\frac{1}{2}\left(\frac{\eta-\eta_o}{\sigma_\eta}\right)^2\right\} \tag{3}$$

where the parameters are given by

$$\begin{aligned} H &= 0.22\ (y_p - y_t - 1.94)\overline{W}\ \ \text{GeV} \\ \eta_o &= 0.74\ \ln\frac{\overline{W}_p}{\overline{W}_t} + 0.30\ (y_p + y_t + 4.3) \\ \sigma_\eta &= 0.20\ (y_p - y_t)\ (1 + \overline{W}^{-0.36}) \end{aligned} \tag{4}$$

The tested limits of applicability of this parameterization are

$$\begin{aligned} 16 &\leq A_p \leq 32 \\ 12 &\leq A_t \leq 197 \\ 10 &\leq \sqrt{s} \leq 20\ \text{GeV} \\ 1.6 &\leq \eta \leq 5.5 \end{aligned} \tag{5}$$

V. References

1 Present address: CERN PPE, Geneva, Switzerland.

2 Present address: KVI, University of Groningen, Groningen, Netherlands.

3 Present address: The Institute for Nuclear Studies, Warsaw, Poland.

4 Present address: Purdue University, West Lafayette, Indiana, USA.

5 The proceedings from the most recent Quark Matter conferences provide an excellent introduction to the field:
QM90, Menton, France, Nucl. Phys. A, in print; QM89, Lenox, USA, Nucl. Phys. **A498** (1989) 1c-628c; QM87, Nordkirchen, FRG, Z. Phys. **C38** 1-370.

6 NA35 Collaboration, A. Bamberger et al., Phys. Lett. **B184** (1987) 271.

7 E802 Collaboration, T. Abbott et al., Phys. Lett. **B197** (1987) 285.

8 WA80 Collaboration, R. Albrecht et al., Phys. Lett. **B199** (1987) 297.

9 NA34 Collaboration, T. Åkesson et al., Z. Phys. **C38** (1988) 383.

10 NA34 Collaboration, T. Åkesson et al., Phys. Lett. **B214** (1988) 295.

11 E814 Collaboration, J. Barrette et al., Phys. Rew. Lett. **64** (1990) 1219.

12 M. J. Tannenbaum, Int. Jour. Mod. Phys **A4** (1989) 3377.

13 J. Stachel, Proc. QM90, Nucl. Phys. A, in print.

14 WA80 Collaboration, R. Albrecht et al., accepted for publication in Phys. Rev. C. Preprints can be obtained by contacting SORENSEN@UTKVX.BITNET.

15 WA80 Collaboration, R. Albrecht et al., Z. Phys. **C45** (1989) 31.

16 C. M. G. Lattes, Phys. Rep. **65** (1980) 151.

17 J. D. Bjorken, Phys. Rev. **D27** (1983) 140.

18 WA80 Collaboration, S. P. Sorensen et al., Z. Phys. **C38** (1988) 3.

DISCLAIMER